

Large-scale simulations of particle-hole-symmetric Pfaffian trial wave functions

Mykhailo Yutushui and David F. Mross

Department of Condensed Matter Physics, Weizmann Institute of Science, Rehovot, 76100, Israel

(Dated: December 30, 2021)

We introduce a family of paired-composite-fermion trial wave functions for any odd Cooper-pair angular momentum. These wave functions are parameter-free and can be efficiently projected into the lowest Landau level. We use large-scale Monte Carlo simulations to study three cases: Firstly, the Moore-Read phase, which serves us as a benchmark. Secondly, we explore the pairing associated with the anti-Pfaffian and the particle-hole-symmetric Pfaffian. Specifically, we assess whether their trial states feature exponentially decaying correlations and thus represent gapped phases of matter. For Moore-Read and anti-Pfaffian we find decay lengths of $\xi_{\text{Moore-Read}} = 1.30(5)$ and $\xi_{\text{anti-Pfaffian}} = 1.38(14)$, in units of the magnetic length. By contrast, for the case of PH-Pfaffian, we find no evidence of a finite length scale for up to 56 particles.

I. INTRODUCTION

The half-filled Landau level is well known for realizing two particularly remarkable manifestations of strong electronic correlations. In the lowest Landau level (LLL) at filling factor $\nu = \frac{1}{2}$, Coulomb interactions between electrons result in a metallic state of emergent charge-neutral quasiparticles.¹⁻⁵ The properties of this state are well described in terms of composite fermions (CFs)—electrons bound to two fictitious flux quanta.⁶⁻⁸ At half-filling, these flux quanta compensate for the magnetic field, and CFs form a gapless “composite Fermi liquid” (CFL).⁹ In the half-filled first excited Landau level, i.e., at $\nu = \frac{5}{2}$, there is instead strong numerical and experimental evidence of a gapped state¹⁰⁻¹⁹ attributed to pairing of composite fermions.²⁰⁻²⁴ The pairing channel is still not fully settled; the leading contenders in numerical studies are the Moore-Read Pfaffian state, which features Cooper pairs with angular momentum $\ell = -1$,^{21,24} and the anti-Pfaffian with $\ell = 3$.^{14,25,26}

A subtle issue in studies of the half-filled Landau level is particle-hole (PH) symmetry, which arises when electrons occupy exactly half of a particular Landau level and interact solely via two-body interactions. Analyses of PH symmetry date back several decades,²⁷ but recent developments have refocused theoretical and experimental efforts on this question. The first of these was a proposal to describe CFs as Dirac particles, on which PH symmetry acts as time-reversal symmetry.²⁸⁻³⁸ The pairing of Dirac CFs is related to one of non-relativistic CFs via $\ell_{\text{Dirac}} = 1 - \ell$. In particular, the unique pairing channel consistent with PH symmetry has $\ell_{\text{Dirac}} = 0$ or $\ell = 1$. The corresponding topological order, irrespective of whether this symmetry is preserved or not, is known as “PH-Pfaffian”.^{28,39-43} To date, there is no known microscopic model that realizes this phase. For the case of Coulomb-interacting electrons at $\nu = \frac{5}{2}$ without Landau-level mixing,¹¹ the numerical findings imply a spontaneously broken PH symmetry.

Experimentally, distinguishing between the possible paired states at $\nu = \frac{5}{2}$ is notoriously difficult because they exhibit the same universal responses to all charge-

sensitive probes. In particular, the Hall conductance $\sigma_{xy} = \frac{5}{2} \frac{e^2}{h}$ is independent of ℓ , as is the elementary quasiparticle charge $e^* = \frac{e}{4}$, measured in Ref. 44. It has long been appreciated that measurements of the thermal Hall conductance κ_{xy} can distinguish between these states, with $\kappa_{xy} = (3 - \frac{\ell}{2}) \frac{\pi k_B}{3h} T$. Such an experiment was recently carried out and, surprisingly, found the value $\ell = 1$ corresponding to PH-Pfaffian.⁴⁵ The marked absence of this phase from all numerical studies has led to proposals that the observed value is either due to disorder-induced formation of the PH-Pfaffian topological order,⁴⁶⁻⁴⁸ or reflects incomplete equilibration between the edge states of an underlying anti-Pfaffian phase.⁴⁹⁻⁵⁴

The numerical search for a realization of the PH-Pfaffian phase in a clean quantum Hall system is considerably impeded by the absence of a trial wave function. A generalization of the celebrated Moore-Read wave function to the PH-Pfaffian phase was proposed in Refs. 55 and 56 (a related wave function was previously introduced in Ref. 57). However, subsequent numerical studies of this state have raised doubts whether it describes a gapped phase or instead represents a gapless CFL.^{58,59}

Specifically, these works observed a substantial overlap between PH-Pfaffian and composite Fermi liquid trial states, as well as pronounced $2k_F$ oscillations in the density-density correlation function. (Within BCS mean-field theory, the amplitude of such oscillations decays exponentially with a length scale set by the inverse superconducting gap.) These analyses were, however, limited to relatively small systems of $N_p = 12$ particles by the need to perform an explicit projection into the LLL. In such small systems, the density-density correlation function exhibits less than two full oscillations. Finite-size effects are thus dominant and the asymptotic decay cannot be determined. In this work, we develop a method of studying PH-Pfaffian trial wave functions for much larger particle numbers and present numerical results for up to $N_p = 56$ particles.

The rest of this paper is organized as follows: In Sec. II, we introduce a family of paired-composite-fermion wave functions for arbitrary odd ℓ , which can be efficiently studied via Monte Carlo methods. This family includes, in particular, the Moore Read ($\ell = -1$), the anti-Pfaffian

($\ell = 3$), and the PH-Pfaffian ($\ell = 1$) states. In Sec. III, we describe and compare several different routes of obtaining LLL wave function from composite-fermion based *Ansätze*. Sec. IV contains our main numerical results. We compute density-density correlation functions of all three states as well as those of unpaired CFLs. We also calculate the overlap between paired and unpaired trial states. In Sec. V, we conclude by discussing the implications of our findings and potential directions in the search for suitable PH-Pfaffian trial states. The Appendices contain additional numerical data and technical details regarding LLL projection.

II. TRIAL WAVE FUNCTIONS OF PAIRED-COMPOSITE FERMIONS

A wide class of paired-composite-fermions wave functions on a sphere was introduced in Refs. 60 and 61 as

$$\Psi_{\text{M\"oller-Simon}} = \mathcal{P}_{\text{LLL}} \left\{ \text{Pf}[g_{ab}] \prod_{a < b} \omega_{ab}^{2p} \right\}, \quad (1)$$

where $\omega_{ab} = u_a v_b - u_b v_a$ with $u = \cos(\frac{\theta}{2}) \exp(i\frac{\phi}{2})$ and $v = \sin(\frac{\theta}{2}) \exp(i\frac{\phi}{2})$. In general, these wave functions require an explicit projection into the LLL, denoted by \mathcal{P}_{LLL} . The Pfaffian factor alone describes a BCS superconductor with Cooper-pair wave function g_{ab} and the Jastrow factor $\prod_{a < b} \omega_{ab}^{2p}$ encodes attachment of $2p$ flux quanta. Instead of the magnetic flux N_ϕ , CFs experience the reduced flux $N_\phi^{\text{eff}} = N_\phi - 2p(N_p - 1)$. Due to the curvature of the sphere, the particle number may be offset from the product of filling factor and magnetic flux by the shift $\mathcal{S} = \nu^{-1}N_p - N_\phi$.⁶² In the half-filled LLL, the effective monopole strength is determined by the shift according to $q \equiv N_\phi^{\text{eff}}/2 = 1 - \mathcal{S}/2$.

In order to specify the pairing channel, we expand g_{ab} in single-particle orbitals corresponding to q , i.e., monopole harmonics $Y_{l,m}^q$.⁶³ (Ref. 60 focused on the Moore-Read case $q_{\text{MR}} = -\frac{1}{2}$. In the context of bilayer systems the case $q = \frac{1}{2}$ was studied in Refs. 60 and 64.) In states with a well-defined Cooper-pair angular momentum $\ell = 2q$, the monopole harmonics enter g_{ab}^ℓ through the linear combinations

$$\Phi_l^q \equiv \sum_m Y_{l,m}^q(r_a) \bar{Y}_{l,m}^q(r_b) = \omega_{ab}^{2q} f_l^q(|\omega_{ab}|), \quad (2)$$

where $\bar{Y}_{l,m}^q \equiv (Y_{l,m}^{-q})^*$ and f_l^q are specified in App. B. (We use ℓ to denote the Cooper-pair angular momentum and l for single-particle orbitals.) A general rotationally symmetric wave function can thus be parametrized as

$$g_{ab}^\ell = \sum_{l \geq |\ell|} \eta_l \Phi_l^q. \quad (3)$$

Different choices of η_l can realize both unpaired and paired states. In the latter cases, the particular choice of η_l does not affect the Cooper-pair angular momentum.

In general, g_{ab}^ℓ contains contributions of electrons in higher Landau levels and, therefore, an explicit LLL projection is required. The contributions from η_l with large l vanish upon projection.⁶⁰ Consequently, the *a priori* infinite number of variational parameters becomes finite and N_p dependent. The remaining η_l can be used to, e.g., optimize the energy of a trial state with respect to a given interaction potential. Conversely, to study specific phases, one needs a prescription for choosing the parameters η_l for any number of particles.

We propose the family of Cooper-pair wave functions,

$$g_{ab}^\ell \equiv \frac{1}{|\omega_{ab}|} e^{i\ell\vartheta_{ab}} = \frac{\omega_{ab}^{q-1/2}}{\bar{\omega}_{ab}^{q+1/2}}, \quad (4)$$

where $\vartheta_{ab} = \arg(\omega_{ab})$. The pairing functions g_{ab}^ℓ have angular momentum ℓ and the characteristic weak-pairing decay $|g_{ab}^\ell| \propto \frac{1}{R}$ at long distances, see also App. A. [In the absence of any length scale, these two properties alone fix the Cooper-pair wave functions to be given by Eq. (4).] They can be brought into the form of Eq. (3) through

$$\frac{\omega_{ab}^{q-1/2}}{\bar{\omega}_{ab}^{q+1/2}} = \sum_{l,m} \frac{8\pi}{2l+1} Y_{l,m}^q(r_a) \bar{Y}_{l,m}^q(r_b). \quad (5)$$

For $q = 0$, this identity reduces to the expansion of the Coulomb potential in spherical harmonics. The $q \neq 0$ case is its generalization to monopole harmonics. We have not seen this expression reported in the literature, but its derivation is straightforward (see App. B).

A. Composite Fermi liquid

The wave function $\Psi_{\text{M\"oller-Simon}}$ of Eq. (1) can describe CFL trial states⁴ for particle numbers that satisfy

$$N_p = \sum_{l=|q|}^{l_F} (2l+1) = (l_F+1)^2 - q^2. \quad (6)$$

If $\eta_l = 0$ for $l > l_F$, the Pfaffian contains precisely as many linearly independent orbitals as particles. Consequently,

$$\Psi_{\text{CFL}}^q \equiv \mathcal{P}_{\text{LLL}} \left\{ \text{Pf} \left[\sum_{l=|q|}^{l_F} \eta_l \Phi_l \right] \prod_{a < b} \omega_{ab}^2 \right\}, \quad (7a)$$

$$\propto \mathcal{P}_{\text{LLL}} \left\{ \det \left[Y_{l_a, m_a}^q(r_b) \right] \prod_{a < b} \omega_{ab}^2 \right\}. \quad (7b)$$

Suppressing η_l with $l > l_F$ forces composite fermions to occupy only states below l_F , i.e., to form a filled Fermi sea. The parameters η_l can thus be used to interpolate between unpaired and paired states.

B. Moore-Read Pfaffian

For the monopole strength $q_{\text{MR}} = -\frac{1}{2}$, the left-hand side of Eq. (5) is $1/\omega_{ab}$ and $\Psi_{\text{M\"oller-Simon}}$ reduces to the

celebrated Moore-Read wave function²¹

$$\Psi_{\text{Moore-Read}} = \mathcal{P}_{\text{LLL}} \left\{ \text{Pf} \left[\frac{1}{\omega_{ab}} \right] \prod_{a<b} \omega_{ab}^2 \right\}. \quad (8)$$

This wave function is already in the LLL, and projection acts trivially. This property is no longer manifest when the argument of the Pfaffian is expanded using Eq. (5); it only holds for the infinite sum. However, the contributions from $l > 2N_p - 3$ vanish upon projection. It follows that $\Psi_{\text{Moore-Read}}$ can be reproduced *exactly* with a *finite* number of parameters $\eta_l = \frac{8\pi}{2l+1}$.

Ref. 60 treated η_l as variational parameters and reported a numerically obtained overlap of over 99% between the Moore-Read and the variational state for $N_p = 20$. That finding was based on a modified form of projection into the lowest Landau level that spoils the exact agreement (see Sec. III A for details). A different implementation of the projection results in the exact Moore-Read wave function (see Sec. III B).

C. Anti-Pfaffian

For monopole strength $q_{\text{aPf}} = \frac{3}{2}$, Eq. (4) describes pairing with angular momentum $\ell = 3$. Composite fermions with this pairing symmetry form the anti-Pfaffian phase. A trial state widely used in exact diagonalization studies is obtained through particle-hole conjugation of the Moore-Read wave function $\Psi_{\text{anti-Pfaffian}} \equiv \Theta \Psi_{\text{Moore-Read}}$. This wave function is, however, not well suited for large-scale Monte Carlo simulations.⁶⁵ Recently, an elaborate parton construction was used to produce an alternative wave function, $\Psi_{\text{anti-Pfaffian}}^{\text{parton}}$, amenable to Monte Carlo methods.⁵⁸ For $N_p = 10$ it exhibits significant overlap 93.8% with $\Psi_{\text{anti-Pfaffian}}$ and the same degeneracies of low-lying states in the entanglement spectrum.

Based on the general family of wave functions defined through Eq. (4), we propose

$$\Psi_{\text{anti-Pfaffian}}^{\text{CF}} = \mathcal{P}_{\text{LLL}} \left\{ \text{Pf} \left[\frac{\omega_{ab}}{\bar{\omega}_{ab}^2} \right] \prod_{a<b} \omega_{ab}^2 \right\}, \quad (9)$$

as an alternative trial state in the anti-Pfaffian phase. In contrast to the Moore-Read case, an explicit projection into the LLL is required here. All efficient algorithms for this purpose that have been developed over the years require that \bar{u} and \bar{v} appear with positive powers,^{7,66–68} which is not the case in Eq. (9). To simulate and analyze $\Psi_{\text{anti-Pfaffian}}^{\text{CF}}$ for large particle numbers, we therefore use the expansion of Eq. (5) with $q_{\text{aPf}} = \frac{3}{2}$. The resulting wave function contains only positive powers of \bar{u} and \bar{v} , more specifically in the form of monopole harmonics. The wave function is thus in a form that can be efficiently projected into the lowest Landau level.

D. Particle-hole-symmetric Pfaffian

For monopole strength $q_{\text{PH}} = \frac{1}{2}$, Eq. (4) describes pairing with angular momentum $\ell = 1$. The corresponding paired-composite-fermion wave function is given by

$$\Psi_{\text{PH-Pfaffian}} = \mathcal{P}_{\text{LLL}} \left\{ \text{Pf} \left[\frac{1}{\bar{\omega}_{ab}} \right] \prod_{a<b} \omega_{ab}^2 \right\}. \quad (10)$$

It was previously proposed in Ref. 55 and studied numerically for $N_p = 10, 12$ in Refs. 58 and 59. These works found indications that projection may result in a state with surprisingly weak (or altogether absent) pairing between composite fermions. Specifically, the overlap between $\Psi_{\text{PH-Pfaffian}}$ and a CFL at the same shift is surprisingly large. For $N_p = 12$ the overlap $|\langle \Psi_{\text{PH-Pfaffian}} | \text{CFL} \rangle| = 95.42(1)\%$ is significantly larger than the one between the Moore-Read state and CFL, $|\langle \Psi_{\text{MR-Pfaffian}} | \text{CFL} \rangle| = 61.9(3)\%$, despite a substantially smaller Hilbert space of the latter.⁵⁹ Moreover, the density-density correlation function of $\Psi_{\text{PH-Pfaffian}}$ features more pronounced $2k_F$ oscillations than $\Psi_{\text{Moore-Read}}$.

As for the case of anti-Pfaffian, the expansion of Eq. (5) provides us with a wave function that can be efficiently projected into the LLL.

III. LOWEST LANDAU-LEVEL PROJECTION

Most of the trial states discussed above do not reside entirely in the LLL. To eliminate contributions from higher Landau levels, one may expand a wave function in single-particle orbitals with well-defined Landau-level index n , and retain only those with $n = 0$. This form of projection was applied to PH-Pfaffian trial states in Refs. 58 and 59, but the exponential increase of the Hilbert-space size quickly renders this approach unfeasible. The same LLL wave function can be obtained by replacing all instances of \bar{u} and \bar{v} with derivatives ∂_u and ∂_v .⁸ However, the number of required derivatives grows rapidly and becomes intractable with modern mathematical software for moderate $N_p \gtrsim 10$. To study larger systems, alternative routes for obtaining LLL wave functions from a given composite-Fermion ansatz have thus been developed.

A. Single-composite-fermion projection

The most widely used projection method was introduced in Ref. 7 based on the ‘‘composite-fermion orbitals’’

$$\mathcal{Y}_{l,m}^q(r_a) = Y_{l,m}^q(r_a) \prod_{b \neq a} \omega_{ab}^p, \quad (11)$$

with $p = 1$ at half-filling. The Pfaffian and Jastrow factor of Eq. (1) can be combined to write the wave function succinctly as

$$\text{Pf}[g_{ab}] \prod_{a<b} \omega_{ab}^2 = \text{Pf} \left[\sum_{l,m} \eta_l \mathcal{Y}_{l,m}^q(r_a) \bar{\mathcal{Y}}_{l,m}^q(r_b) \right]. \quad (12)$$

Table I. Single and pairwise projections of Eq. (15) for $N_p = 56$ are well converged at cutoff $N_c \equiv l_c - |q| = 14$. The latter becomes indistinguishable from $\Psi_{\text{Moore-Read}}$ within double precision for $N_c \approx 18$ and matches exactly for $N_c \geq 55$.

	$N_c = 8$	$N_c = 10$	$N_c = 15$	$N_c = 20$
$ \langle \Psi_{\text{MR}} \Psi_{\text{MR},l_c}^{\text{pair}} \rangle $	95.4(3)%	98.48(6)%	99.995(1)%	100(0)%
$ \langle \Psi_{\text{MR}} \Psi_{\text{MR},l_c}^{\text{single}} \rangle $	77.2(6)%	95.4(2)%	93.3(2)%	93.3(2)%

Here, $\bar{\mathcal{Y}}$ is defined as complex conjugation of the monopole harmonic, but not of the ω^p factor.

One can now define “single-composite-fermion projection” as separately projecting each CF orbital, i.e.,

$$\mathcal{P}_{\text{LLL}}^{\text{single}} \text{Pf}[\dots] \equiv \text{Pf} \left[\sum_{l,m} \eta_l \mathcal{P}_{\text{LLL}} \mathcal{Y}_{l,m}^q(r_a) \mathcal{P}_{\text{LLL}} \bar{\mathcal{Y}}_{l,m}^q(r_b) \right]. \quad (13)$$

Algorithms for the efficient evaluation of the projected composite-fermion orbitals were described in Ref. 7 and further refined in Refs. 66–68.

B. Pairwise composite fermion projection

The form of the wave function in Eq. (12) suggests projecting the argument of the Pfaffian as a whole, rather than individual \mathcal{Y} . We thus define “pairwise-composite-fermion projection” as

$$\mathcal{P}_{\text{LLL}}^{\text{pair}} \text{Pf}[\dots] \equiv \text{Pf} \left[\sum_{l,m} \eta_l \mathcal{P}_{\text{LLL}} \{ \mathcal{Y}_{l,m}^q(r_a) \bar{\mathcal{Y}}_{l,m}^q(r_b) \} \right]. \quad (14)$$

This form of projection may be implemented similarly to single CF projection and with comparable efficiency. (When using the algorithms described in Refs. 67 and 68, we find pairwise projection to be moderately faster.) In App. C, we describe this approach in detail.

C. Comparison of different projection methods

Wave functions projected with either \mathcal{P}_{LLL} , $\mathcal{P}_{\text{LLL}}^{\text{single}}$, or $\mathcal{P}_{\text{LLL}}^{\text{pair}}$ do not, in general, coincide. However, in most cases, they describe the same topological phase, which can be inferred, e.g., from their entanglement spectra. It is thus often justified to adopt single or pairwise projection to access large system sizes.

To illustrate the different projection methods, consider the (unprojected) wave function

$$\Psi_{l_c}^q = \text{Pf} \left[\sum_{l=|q|}^{l_c} \frac{8\pi}{2l+1} \sum_m \mathcal{Y}_{l,m}^q(r_a) \bar{\mathcal{Y}}_{l,m}^q(r_b) \right]. \quad (15)$$

For q_{MR} and cutoff $l_c = \infty$ ⁶⁹, it coincides with $\Psi_{\text{Moore-Read}}$, and the argument of the Pfaffian lies in the LLL. Consequently, both \mathcal{P}_{LLL} and $\mathcal{P}_{\text{LLL}}^{\text{pair}}$ act trivially. At

Table II. Single and pairwise projections of CFLs at q_{MR} yield strikingly different overlaps with $\Psi_{\text{Moore-Read}}$. At q_{PH} , the overlap between CFL and Ψ_{PH} is substantial, independent of the projection method.

	$N_p = 12$	$N_p = 30$	$N_p = 42$	$N_p = 56$
$ \langle \Psi_{\text{PH}}^{\text{pair}} \Psi_{\text{CFL}}^{\text{single}} \rangle $	95.8(1)%	66.7(1)%	46.2(1)%	28.7(1)%
$ \langle \Psi_{\text{MR}} \Psi_{\text{CFL}}^{\text{single}} \rangle $	57.5(1)%	13.2(2)%	4.8(5)%	1.3(1)%
$ \langle \Psi_{\text{MR}} \Psi_{\text{CFL}}^{\text{pair}} \rangle $	97.9(1)%	94.4(2)%	91.9(4)%	89.6(4)%

finite l_c , the argument contains contributions from higher Landau levels. Still, for $l_c > 2N_p - 3$ and $l_c > N_p - 1$, the Moore-Read wave function is reproduced exactly by \mathcal{P}_{LLL} and $\mathcal{P}_{\text{LLL}}^{\text{pair}}$. Contributions from larger l vanish under projection.⁷ By contrast, single-composite-fermion projection applies to each orbital separately and thus acts non-trivially for any l_c . In practice, both single and pairwise projections well approximate $\Psi_{\text{Moore-Read}}$ already at $l_c \approx 2l_F \approx 2\sqrt{N_p}$, (see Tab. I).

For q_{aPf} and q_{PH} , we find that $\mathcal{P}_{\text{LLL}}^{\text{single}}$ and $\mathcal{P}_{\text{LLL}}^{\text{pair}}$ yield wave functions that are almost independent of l_c beyond $2l_F$ (see App. E for data at q_{PH}). This rapid convergence makes the expansion attractive for numerical simulations.

There are, however, instances where different types of projection yields dramatically different results. A striking example is given by the CFL at q_{MR} , which arises for $l_c = l_F$ [see also Eq. (7)]. Here, \mathcal{P}_{LLL} and $\mathcal{P}_{\text{LLL}}^{\text{single}}$ produce the expected gapless states; for $N_p = 12$, their overlaps with $\Psi_{\text{Moore-Read}}$ are 61.9(3)% and 57.5(1)%, respectively. When using pairwise projection, we instead find a state with a much larger overlap of 97.9(1)% and an entanglement spectrum matching that of $\Psi_{\text{Moore-Read}}$. For larger N_p , the margin between two projection schemes grows rapidly (see Table II). By contrast, for CFLs at positive q , single and pairwise projections are identical. We therefore use single-composite-fermion projection (the Jain-Kamilla method) for CFLs at any q .

The example of the CFL at q_{MR} illustrates that wave functions obtained through different projection schemes need not even belong to the same phase. In cases such as PH-Pfaffian, where projection yields unexpected results,^{58,59} it may be prudent to compare different methods. Fortunately, this is *not* the “typical” behavior, and in the case of PH-Pfaffian, we do not find significant differences between trial states projected with either method.

IV. NUMERICAL RESULTS

The primary motivation for this work is to determine whether the PH-Pfaffian wave function represents a gapped phase. Since we are studying properties of trial states rather than Hamiltonians, we use a finite correlation length ξ as a proxy for the (inverse) gap. Using Monte Carlo simulation, we compute the normalized

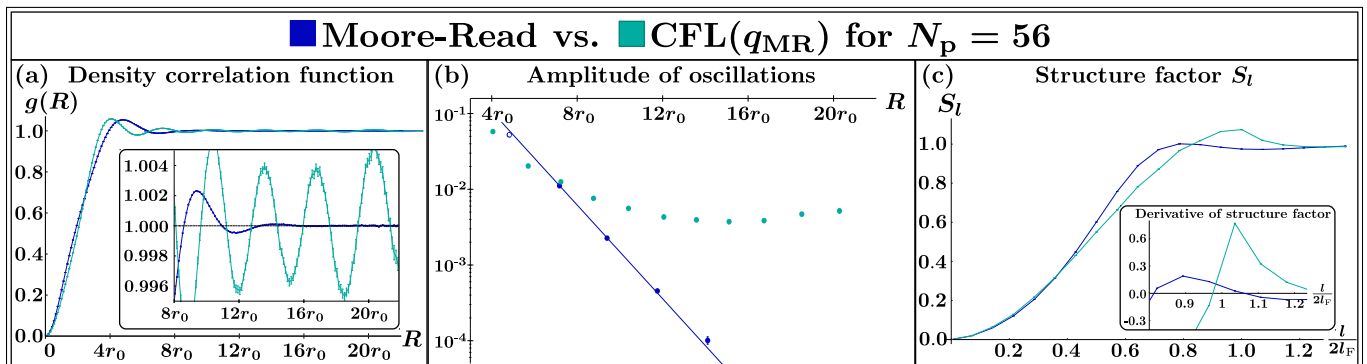


Figure 1. (a) The density-density correlation function of the Moore-Read state exhibits $2k_F$ oscillations that decay very rapidly with the arc length R . In the CFL, by contrast, oscillations persist across the entire sphere. (b) A semilogarithmic plot of the oscillation amplitude shows their exponential decay in the Moore-Read case. The straight line represents a fit to a decay length $\xi \approx 1.46r_0$, where the maximum near the typical inter-particle distance $R = 4r_0$ is viewed as encoding short-distance properties and thus excluded. The amplitude for the CFL decays much slower than exponentially. (c) The static structure factor of the Moore-Read state is smooth for all l , while that of the CFL exhibits a sharp cusp at $2l_F$, indicating a power-law decay of real-space oscillations.

density-density correlation function on a unit sphere

$$g(R) = \frac{1}{N_p^2} \sum_{a \neq b} \langle \delta[\mathbf{r}_a \cdot \mathbf{r}_b - \cos(R)] \rangle, \quad (16)$$

where $\mathbf{r}_{a,b}$ are particle positions, and R is the arc distance. The natural length scale is $r_0 = N_p^{-1/2}$, the magnetic length at half-filling. (For circular Fermi surfaces, r_0 coincides with k_F^{-1} dictated by Luttinger's theorem). In parallel, we compute the static structure factor⁷⁰

$$S_l = 1 + \frac{1}{N_p} \sum_{a \neq b} \langle P_l(\mathbf{r}_a \cdot \mathbf{r}_b) \rangle, \quad (17)$$

where $P_l(x)$ are Legendre polynomials.

In a Fermi liquid, the structure factor is non-analytic near $2l_F$, i.e., $S_{2l_F+\delta l} - S_{2l_F} \propto (\delta l)^{\alpha-3/2}$ with $\alpha_{FL} = 3$. This singularity is reflected in a slow decay of $2k_F$ oscillations in real space, i.e., $g(R) \propto \cos(2k_F R)/R^\alpha$ at long distances $\sqrt{N_p} \gg R/r_0 \gg 1$. In a spherical geometry, the oscillation amplitude increases as $R \rightarrow \pi$ due to constructive interference between different quasiparticle paths (see also App. D).

In strongly correlated metals with poorly defined quasiparticles, the exponent governing this decay can change, but power-law oscillations may persist even when quasiparticles become poorly defined.^{71,72} The presence of such oscillations is thus a useful numerical probe of emergent Fermi surfaces in quantum Hall systems and spin liquids.^{31,73} When pairing gaps out the Fermi surface, the oscillations decay exponentially with a length scale $\xi_{2k_F} \propto \Delta_{\text{pair}}^{-1}$.

A. Moore-Read Pfaffian

We begin our numerical analysis by revisiting the well-studied Moore-Read state. Specifically, we use a stan-

dard Monte Carlo algorithm to compute the density-density correlation function and the structure factor for the Moore-Read state and the CFL at the same monopole strength. Their behavior is well understood; we still reproduce them here as context for our subsequent analysis of the anti-Pfaffian and PH-Pfaffian states. To facilitate the comparison, we focus on particle numbers accessible for three states and that permit CFLs with filled shells, [cf. Eq. (6)].

In Fig. 1(a), we show the density-density correlations for $N_p = 56$. In the Moore-Read state, the initial oscillations decay rapidly, and $g(R)$ quickly approaches unity. A semilogarithmic plot of the oscillation amplitudes shows the exponential decay expected for a paired state [Fig. 1(b)]. We fit the decay lengths for the Moore-Read state with $N_p = 20, 30, 42, 56, 72$ and extrapolate to the thermodynamic limit, where we find $\xi_{MR} = 1.30(5)r_0$. This result is consistent with the value $\xi_\psi \approx 1.3r_0$, extracted in Ref. 74 and 75 from the neutral fermion gap through exact diagonalization of Coulomb interactions. A somewhat longer length scale $\xi_{\text{split}} \approx 2.3r_0$ was obtained in Ref. 76 for the finite-size splitting between two putatively degenerate ground states.

In Fig. 1(c), we show the static structure factors. For the Moore-Read state, S_l is smooth around $2l_F$. By contrast, it exhibits a cusp in the case of the CFL, consistent with the slow decay of real-space oscillations. Unfortunately, there is less than a decade between the short-distance peak near $R = 4r_0$ and the onset of strong finite-size effects. Consequently, the exponent α cannot be obtained with confidence, and values in the range 2–2.8 are consistent with the data shown in Fig 1. Ref. 77 reported a best-fit value of $\alpha \approx 2.75$ for CFLs with $N_p = 54$ particles at monopole strength $q_{\text{aPf}} = 3/2$.

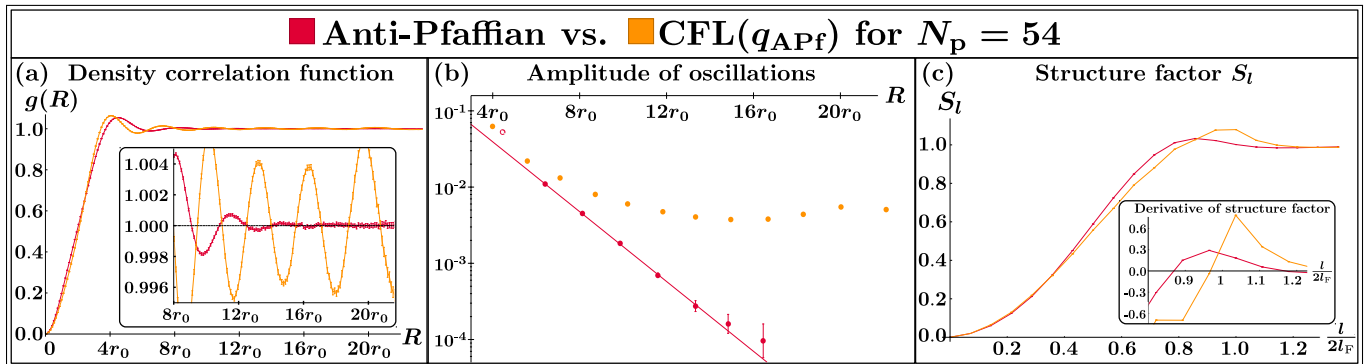


Figure 2. (a) The density-density correlation functions of the anti-Pfaffian and CFL trial states qualitatively match their analogs at q_{MR} , (cf. Fig. 1). (b) The $2k_F$ oscillations decay exponentially with a length $\xi \approx 1.9r_0$ for the anti-Pfaffian state but much slower for the CFL. As before, the $R \approx 4r_0$ peak is excluded from the fit. (c) The anti-Pfaffian structure factor is smooth, while that of the CFL exhibits a cusp at $2l_F$, similar to the one in Fig. 1(c).

B. Anti-Pfaffian

We now analyze the anti-Pfaffian trial state introduced in Sec. III C. As a first step, we compute its overlap with the explicit particle-hole conjugate of the Moore-Read state. The shifts of the two states imply that $\Psi_{\text{anti-Pfaffian}}(N_p) = \hat{\Theta} \Psi_{\text{Moore-Read}}(N_p + 2)$. Due to the exponential growth of the Hilbert space, we are only able to make an accurate comparison for up to ten particles. Tab. III lists the overlaps between $\Psi_{\text{anti-Pfaffian}}$ and $\Psi_{\text{anti-Pfaffian}}^{\text{CF}}$ for any of the three projection methods described in Sec. III. We find a remarkably large overlap above 99% for two of the projections schemes. Unsurprisingly, the low-lying states in the entanglement spectrum agree even quantitatively (see App. F).

We now turn to a larger system of $N_p = 54$, where a CFL with filled shells up to $l_F = 13/2$ is also possible [cf. Eq. (6)]. Here, only single and pairwise projections are applicable; we do not find significant differences between the two and quote numbers using the latter. We find the overlap between the anti-Pfaffian and CFL trial states to be 6.84(2)%. To compare this value to its analogue at the Moore-Read shift, one may look at states with the same Hilbert space size ($N_p = 56$) or with the same l_F ($N_p = 42$). These overlaps are 1.3(1)% and 4.8(5)%, respectively, comparable to those for the anti-Pfaffian.

Next, we compute the density-density correlations for anti-Pfaffian and CFL at $N_p = 54$. Our results are shown in Fig. 2; they closely mirror those of the Moore-Read state. For the anti-Pfaffian trial state, we find an exponential decay of oscillations and a smooth structure factor. We extract the correlation length for $N_p = 28, 40, 54$ and extrapolate to the thermodynamic limit, where we find $\xi_{\text{aPf}} = 1.38(14)r_0$, close to $\xi_{\text{MR}} = 1.30(5)r_0$. The CFL wave function at the anti-Pfaffian shift behaves very similarly to the one at the Moore-Read shift, i.e., it exhibits a much slower decay of oscillations and a cusp at $2l_F$ in the structure factor.

Table III. The anti-Pfaffian wave function Eq. (9) has a large overlap with the PH-conjugate of the Moore-Read state for $N_p = 6, 8, 10$. The values for $\Psi_{\text{anti-Pfaffian}}^{\text{parton}}$ are from Ref. 58.

Wave function	$N_p = 6$	$N_p = 8$	$N_p = 10$
$\Psi_{\text{anti-Pfaffian}}^{\text{CF}}$	99.407(1)%	99.31(6)%	99.11(28)%
$\Psi_{\text{anti-Pfaffian}}^{\text{CF, single}}$	99.260(18)%	99.36(8)%	99.12(16)%
$\Psi_{\text{anti-Pfaffian}}^{\text{CF, pair}}$	97.925(6)%	98.20(9)%	95.99(14)%
$\Psi_{\text{anti-Pfaffian}}^{\text{parton}}$	96.86%	95.23%	93.97%

Our findings provide strong evidence that the trial state $\Psi_{\text{anti-Pfaffian}}^{\text{CF}}$ can describe the anti-Pfaffian phase for large N_p . Its high overlap with the particle-hole conjugate of Ψ_{MR} at moderate N_p suggests that it may, moreover, be useful for addressing certain questions related to particle-hole symmetry. For example, the variational energies in the presence of three-body interactions (which can be attributed to Landau-level mixing) for Moore-Read and anti-Pfaffian states could be meaningfully compared.

C. PH-Pfaffian

We begin our analysis of the PH-Pfaffian trial state by comparing the projection methods described in Sec. III at small particle numbers. Up to $N_p = 12$, all three projection methods are applicable and give similar results. The overlap between Ψ_{PH} and its pairwise projected version is 99.2(5)%, somewhat larger than for single CF projection where we find 98.7(7)%. The overlap of all three states with the CFL is around 95%. For larger systems where only single and pairwise projection are feasible, we find no appreciable difference between the two, and that retaining CF Landau levels up to $2l_F$ is sufficient (see. App. E). We therefore simply refer to $\Psi_{\text{PH}}^{\text{pair}}$ at this cutoff as ‘the PH-Pfaffian trial state.’ For $N_p = 56$, we

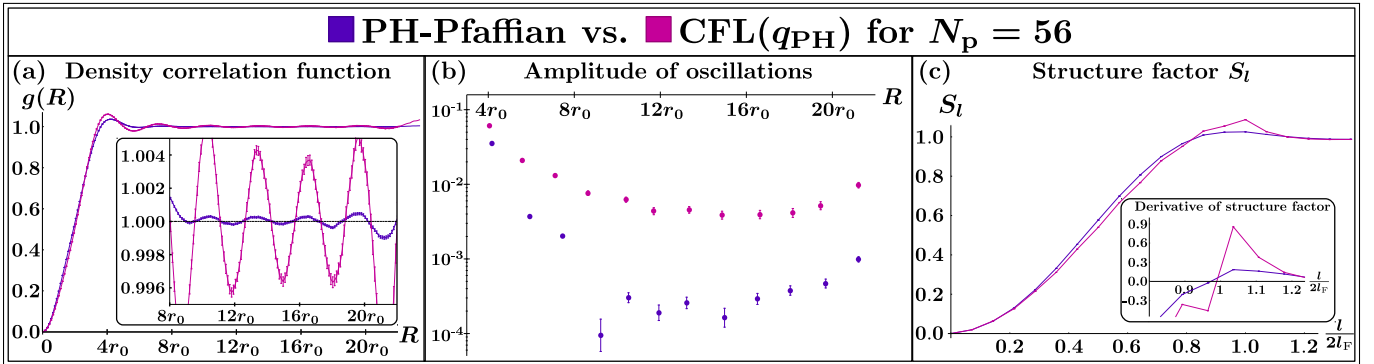


Figure 3. (a) Both the PH-Pfaffian trial state and the corresponding CFL exhibit slowly decaying $2k_F$ oscillations, with approximately the same wavelength. The overall amplitude of these oscillations is an order of magnitude smaller for PH-Pfaffian. (b) A semilogarithmic plot shows that the PH-Pfaffian oscillations are inconsistent with an exponential decay and instead behave similarly to those of the CFL. (c) The structure factor of the PH-Pfaffian state has a small cusp around $2l_F$, unlike those of Moore-Read and anti-Pfaffian.

find that its overlap with the CFL is still 28.65(3)%, significantly larger than in the Moore-Read case where the analogous overlap is 1.3(1)%.

Next, we compute the density-density correlation functions for the PH-Pfaffian trial state and the CFL at the same shift (see Fig. 3). We find that the $2k_F$ oscillations of both states persist across the entire system [Fig. 3(a)]. The non-universal *overall* amplitude of oscillations is significantly smaller for the PH-Pfaffian trial state than for the CFL by an R -independent factor [Fig. 3(b)]. (In a Fermi liquid, such an R -independent change of oscillation amplitudes may originate in a different quasiparticle weight.) The relatively weak oscillations are reflected in a rather faint cusp in S_l [Fig. 3(c)]. Notice, however, that both the PH-Pfaffian and the CFL trial states exhibit a peak in $\partial_l S_l$ at the same $l \approx 2l_F$ —unlike the Moore-Read and anti-Pfaffian cases shown in Figs. 1(c) and 2(c). These observations strongly suggest that both wave functions lie in the same gapless CFL phase.

Finally, we perform a simple test of the relationship between the loss of a pairing gap and PH symmetry. We study the PH-Pfaffian trial state adapted to the filling factor $\nu = \frac{1}{4}$, where the question of PH symmetry does not arise. A possible trial wave function at this filling can be easily obtained by multiplying a $\nu = \frac{1}{2}$ wave function with a suitable Jastrow factor. However, such a wave function would presumably inherit many of the latter's properties, including any suppression of the gap. We instead choose $p = 2$ in Eq. (11) and proceed with projection as described in Sec. III. We find $2k_F$ oscillations that persist over the entire system for the largest system sizes that we studied ($N_p = 30$); see App. E for details. This finding indicates that the obliteration of the gap due to projection is not necessarily related to PH symmetry, but this connection deserves a more systematic study.

V. SUMMARY AND CONCLUSIONS

We have studied a class of paired-composite-fermions trial wave functions at filling factors $\nu = \frac{1}{2p}$. These wave functions can be efficiently projected into the LLL for any odd Cooper-pair angular momentum ℓ . For $\ell = -1$, the Moore-Read wave function is reproduced exactly, which serves as a useful benchmark for subsequent approximations. The case $\ell = 3$ describes a wave function in the anti-Pfaffian phase that, for moderate particle numbers, well approximates the particle-hole conjugate of the Moore-Read Pfaffian. This wave function may be useful in future comparative studies between these two phases, e.g., in the presence of Landau-level mixing.

The $\ell = 1$ member of this family has been previously proposed to lie in the PH-Pfaffian phase.⁵⁵ We have simulated this trial state at $\nu = \frac{1}{2}$ for relatively large system sizes of up to $N_p = 56$ and found no evidence of a pairing gap on the composite-Fermi surface. To test for a possible relationship between the loss of a gap and PH symmetry, we further studied PH-Pfaffian states at $\nu = \frac{1}{4}$, and found similar behavior to the half-filled case.

The variational freedom afforded by the wave function of Eq. (1) may well permit a fully gapped PH-Pfaffian phase in the lowest Landau level. We note that a pure power-law dependence $\eta_l \sim l^{-1+\gamma}$ in Eq. (2) corresponds to a Cooper-pair wave function $g(R) \sim R^{-1-\gamma}$ for $\gamma \in [0, 1]$. Insisting on weak-pairing behavior of the unprojected wave function fixes $\gamma = 0$ and a scale-dependent choice of the parameters η_l is required to access different states. Here, l_F constitutes the only available scale, and larger values η_l for $l > l_F$ promote pairing correlations. For the *projected* wave function, we have found that only parameters with $l \leq 2l_F$ play a significant role. There are consequently a relatively small number of variational parameters, and it would be interesting to explore whether they permit access to the fully gapped PH-Pfaffian phase.

Finally, we have observed that different means of pro-

jecting the same CF ansatz can result in LLL wave functions that describe altogether different phases of matter. Depending on the specific trial state and the purpose of the study, either method may be preferable. The pairwise projection method introduced here provides an alternative to the widely used single CF projection and is, likewise, suitable for large-scale Monte Carlo simulations.

ACKNOWLEDGMENTS

It is a pleasure to thank Jason Alicea, Tobias Holder, Ryan Mishmash, and Olexei I. Motrunich for illuminating discussions. This work was supported by the Israel Science Foundation (ISF) and the Minerva Foundation with funding from the Federal German Ministry for Education and Research.

Appendix A: Mean-field-superconductor wave function

The wave functions of spinless mean-field superconductors can be constructed as prescribed in Ref. 24. Consider a model of spinless fermions in two dimensions with a mean-field pairing term, i.e.,

$$H_{\text{BCS}} = \sum_{\mathbf{k}} \left[\xi_{\mathbf{k}} c_{\mathbf{k}}^{\dagger} c_{\mathbf{k}} + \frac{1}{2} (\Delta_{\mathbf{k}}^* c_{-\mathbf{k}} c_{\mathbf{k}} + \text{H.c.}) \right]. \quad (\text{A1})$$

The Hamiltonian H_{BCS} is diagonalized by the Bogoliubov transformation $a_{\mathbf{k}} = u_{\mathbf{k}} c_{\mathbf{k}} - v_{\mathbf{k}} c_{-\mathbf{k}}^{\dagger}$, i.e.,

$$H_{\text{BCS}} = \sum_{\mathbf{k}} E_{\mathbf{k}} a_{\mathbf{k}}^{\dagger} a_{\mathbf{k}}, \quad E_{\mathbf{k}} = \sqrt{\xi_{\mathbf{k}}^2 + |\Delta_{\mathbf{k}}|^2}. \quad (\text{A2})$$

The functions $u_{\mathbf{k}}$ and $v_{\mathbf{k}}$ (not to be confused with the coordinates u_a, v_a) satisfy $|u_{\mathbf{k}}|^2 + |v_{\mathbf{k}}|^2 = 1$ and

$$g_{\mathbf{k}} \equiv \frac{v_{\mathbf{k}}}{u_{\mathbf{k}}} = \frac{\xi_{\mathbf{k}} - E_{\mathbf{k}}}{\Delta_{\mathbf{k}}^*}. \quad (\text{A3})$$

The ground state $|\Omega\rangle$ of H_{BCS} satisfies $a_{\mathbf{k}}|\Omega\rangle = 0$ for all \mathbf{k} ; in terms of the original fermions $c_{\mathbf{k}}^{\dagger}$ it is

$$|\Omega\rangle \propto \exp \left[\frac{1}{2} \sum_{\mathbf{k}} g_{\mathbf{k}} c_{\mathbf{k}}^{\dagger} c_{-\mathbf{k}}^{\dagger} \right] |0\rangle. \quad (\text{A4})$$

The corresponding real-space wave function for an even number of fermions is given by

$$\Psi(\mathbf{r}_1, \dots, \mathbf{r}_{N_p}) = \text{Pf}[g(\mathbf{r}_a - \mathbf{r}_b)], \quad (\text{A5})$$

where $g(\mathbf{r})$ is the Fourier transform of $g_{\mathbf{k}}$.

For spinless fermions, $\Delta_{\mathbf{k}}$ must be an odd function of \mathbf{k} and, in particular, vanishes at $\mathbf{k} = 0$. Thus, we consider pairing with odd angular momentum ℓ , i.e., $\Delta_{\mathbf{k}} = \Delta|\mathbf{k}|e^{i\ell\vartheta_{\mathbf{k}}}$, where $\vartheta_{\mathbf{k}}$ is the angle between \mathbf{k} and the x -axis. Using Eq. (A3), one finds $\lim_{|\mathbf{k}| \rightarrow 0} g_{\mathbf{k}} = -\frac{2\mu}{\Delta_{\mathbf{k}}}$

for positive chemical potential. The choice of $\Delta_{\mathbf{k}}$ above results in $g_{\mathbf{k}} \sim -\frac{2\mu}{\Delta} \frac{1}{|\mathbf{k}|} e^{i\ell\vartheta_{\mathbf{k}}}$ and the Fourier transform

$$g(\mathbf{r}) = -i^{\ell} e^{i\ell\vartheta_{\mathbf{r}}} \int dk k |g_{\mathbf{k}}| J_{\ell}(kr), \quad (\text{A6})$$

where J_{ℓ} is the Bessel function of the first kind, which satisfies the normalization $\int_0^{\infty} dx J_{\ell}(x) = 1$. The momentum integral converges rapidly enough that it suffices to insert the small- \mathbf{k} limit of $g_{\mathbf{k}}$. We thus find

$$g(\mathbf{r}) \approx \frac{2\mu}{\Delta} \frac{-i^{\ell}}{|\mathbf{r}|} e^{i\ell\vartheta_{\mathbf{r}}}, \quad (\text{A7})$$

precisely the pair wave function in Eq. (5).

Appendix B: Expansion of Cooper pair wavefunction in monopole harmonics

To derive Eq. (5), first start with the addition theorem for monopole harmonics, Refs. 78 and 79, which can be expressed as

$$\sum_{m=-l}^l Y_{l,m}^q(\mathbf{r}_a) \bar{Y}_{l,m}^q(\mathbf{r}_b) = \sqrt{\frac{2l+1}{4\pi}} Y_{l,q}^q(\theta, \phi=0) F_q(\mathbf{r}_a, \mathbf{r}_b). \quad (\text{B1})$$

Here the angle θ is given by $\mathbf{r}_a \cdot \mathbf{r}_b = \cos \theta = 1 - 2|\omega_{ab}|^2$ and $F_q(\mathbf{r}_a, \mathbf{r}_b)$ is a phase factor that does not depend on the Landau-level index $l - q$. To determine this factor, it is sufficient to focus on the LLL, $l = q$, where considerable simplifications occur. Specifically, for positive q the monopole harmonics satisfy

$$Y_{q,m}^q(\mathbf{r}_a) \bar{Y}_{q,m}^q(\mathbf{r}_b) = \frac{2q+1}{4\pi} \binom{2q}{q-m} (u_a v_b)^{q-m} (u_b v_a)^{q+m}, \quad (\text{B2})$$

and thus

$$\sum_{m=-q}^q Y_{q,m}^q(\mathbf{r}_a) \bar{Y}_{q,m}^q(\mathbf{r}_b) = \frac{2q+1}{4\pi} (u_a v_b - u_b v_a)^{2q}. \quad (\text{B3})$$

Inserting this phase factor into Eq. (B1) yields

$$\sum_{m=-l}^l Y_{l,m}^q(\mathbf{r}_a) \bar{Y}_{l,m}^q(\mathbf{r}_b) = \frac{2l+1}{4\pi} \omega_{ab}^{2q} P_{l-q}^{(2q,0)}(\cos \theta), \quad (\text{B4})$$

where $P_n^{(2q,0)}$ are Jacobi polynomials, which satisfy

$$\frac{1}{|\omega_{ab}|^{2q+1}} = 2 \sum_{n=0}^{\infty} P_n^{(2q,0)}(\cos \theta). \quad (\text{B5})$$

(This relation follows directly from the generation functional). Multiplying Eq. (B5) with ω_{ab}^{2q} and using Eq. (B4), we arrive at the relation quoted in the main

text, i.e.,

$$\frac{\omega_{ab}^{q-1/2}}{\bar{\omega}_{ab}^{q+1/2}} = 2\omega_{ab}^{2q} \sum_{n=0}^{\infty} P_n^{(2q,0)}(1-2|\omega_{ab}|^2) \quad (\text{B6a})$$

$$= \sum_{l=|q|}^{\infty} \frac{8\pi}{2l+1} \sum_{m=-l}^l Y_{l,m}^q(\mathbf{r}_a) \bar{Y}_{l,m}^q(\mathbf{r}_b). \quad (\text{B6b})$$

Using complex conjugation and symmetries of the monopole harmonics, one finds that Eq. (B6b) also holds for negative monopole strength q .

Appendix C: Details on pairwise projection

Any spherically symmetric composite-fermion-pair wave function that may appear in the argument of the Pfaffian in Eq. (12) can be expressed using Eq. (B4) as

$$g_{ab}^{\text{CF}} = \sum_n C_n \bar{\omega}_{ab}^n \omega_{ab}^n \Phi^Q, \quad (\text{C1})$$

where Φ^Q is a LLL wave function at monopole strength $Q > 0$. This function can be projected by replacing $\bar{\omega}_{ab}$ with the differential operator $\hat{d}_{ab} \equiv \partial_{u_a} \partial_{v_b} - \partial_{u_b} \partial_{v_a}$, i.e.,

$$\mathcal{P}_{\text{LLL}} \{ \bar{\omega}_{ab}^n \omega_{ab}^n \Phi^Q \} = \left[\frac{(2Q+1)!}{(2Q+n+1)!} \right]^2 \hat{d}_{ab}^n \omega_{ab}^n \Phi^Q. \quad (\text{C2})$$

To commute all d_{ab} to the right of all ω_{ab} , we introduce the operator $\hat{t}_{ab} \equiv u_a \partial_{u_a} + v_a \partial_{v_a} + u_b \partial_{u_b} + v_b \partial_{v_b}$, which satisfies $\hat{t} \Phi^Q = 4Q \Phi^Q$. Moreover, \hat{d} , \hat{t} , and ω form a closed algebra

$$[\hat{d}, \omega] = \hat{t} + 2, \quad [\hat{t}, \omega] = 2\omega, \quad [\hat{t}, \hat{d}] = -2\hat{d}. \quad (\text{C3})$$

[This is a representation of $SU(2)$ with the identification $L_+ = \omega$, $L_- = -\hat{d}$, and $L_z = \frac{\hat{t}+2}{2}$]. After a straightforward calculation, we find

$$\hat{d}^s \omega^n = \sum_{k=0}^{\min\{n,s\}} \frac{n!s!}{k!} \frac{\omega^{n-k}}{(n-k)!} \frac{\hat{d}^{s-k}}{(s-k)!} \hat{f}_k^{n-s}, \quad (\text{C4})$$

where $\hat{f}_k^\delta \equiv \prod_{i=1}^k (\hat{t} + i + \delta + 1)$. For CFs at filling factor $\nu = 1/2p$, the function Φ^Q is given by

$$\Phi^Q = \omega_{ab}^{2p+2q} \mathcal{J}_{ab}^p \equiv \omega_{ab}^{2p+2q} \left(\prod_{i \neq a,b} \omega_{ai} \omega_{bi} \right)^p. \quad (\text{C5})$$

To perform projection, one still needs to compute the derivatives $d_{ab}^n \mathcal{J}_{ab}^p$. In the case $p = 1$ the expressions simplify considerably. We observe that

$$\hat{d}_{ab}(\omega_{ai} \omega_{bj}) = \omega_{ij} = \Omega_{ij} \omega_{ai} \omega_{bj}, \quad \Omega_{ij} \equiv \frac{\omega_{ij}}{\omega_{ai} \omega_{bj}}, \quad (\text{C6})$$

and compute

$$\begin{aligned} \hat{d}_{ab} \mathcal{J}_{ab} &= \hat{d}_{ab} \left(\prod_i' \omega_{ai} \omega_{bi} \right) = \mathcal{J}_{ab} \sum_{i,j}' \Omega_{i,j} \\ &= \sum_{i,j} \omega_{ij} \left(\prod_{k \neq i, l \neq j}' \omega_{ak} \omega_{bl} \right). \end{aligned} \quad (\text{C7})$$

Here, the prime specifies that indices run over all particles other than a and b . Notice that the product in the last line of Eq. (C7) has a similar structure as \mathcal{J}_{ab} . Consequently, acting repeatedly with \hat{d}_{ab} results in

$$\hat{d}_{ab}^n \mathcal{J}_{ab} = \mathcal{J}_{ab} \sum_{i_1 \neq \dots i_n} \sum_{j_1 \neq \dots j_n} \prod_{\alpha=1}^n \Omega_{i_\alpha j_\alpha}. \quad (\text{C8})$$

Next, we introduce $h_i^{ab} = \omega_{ai} / \omega_{bi}$ to rewrite

$$\omega_{ab} \Omega_{ij} = 1 - h_i^{ab} h_j^{ba}. \quad (\text{C9})$$

As a final step, we multiply Eq. (C8) by ω_{ab}^n and use Eq. (C9) to find

$$\omega_{ab}^n \hat{d}_{ab}^n \mathcal{J}_{ab} = \sum_{k=0}^n (-1)^k \binom{n}{k} \left(\frac{k!(N-k)!}{(N-n)!} \right)^2 \mathcal{J}_{ab} e_k^{ab} e_k^{ba}. \quad (\text{C10})$$

Here $N = N_p - 2$ and e_k^{ab} are the elementary symmetric polynomial in N variables h_i for $i \neq a, b$, i.e.,

$$e_k^{ab}(\{h_j^{ab}\}) = \sum_{i_1 < \dots < i_k} \prod_{\alpha=1}^k h_{i_\alpha}^{ab}. \quad (\text{C11})$$

A straightforward evaluation of these sums would require on the order of N_p^n operations, but can fortunately be avoided. Refs. 66–68 developed an efficient algorithm for evaluating e_n^{ab} , which can be readily adapted to the present case.⁸⁰ In our simulations we further use the library of Ref. 81 for efficiently evaluating Pfaffians.

For the wave functions introduced in the main text, the steps described by Eqs.(C1)–(C4) result in

$$\mathcal{P}_{\text{LLL}} \left[\frac{\omega_{ab}^{q-1/2}}{\bar{\omega}_{ab}^{q+1/2}} \omega_{ab}^{2p} \mathcal{J}_{ab}^p \right]_{N_c} = \sum_{n=0}^{N_c} A_n^{N_c} \omega_{ab}^{n+2p+2q} d_{ab}^n \mathcal{J}_{ab}^p, \quad (\text{C12})$$

where $N_c = l_c - |q|$ is the cutoff [cf. Eq. (15)], and the

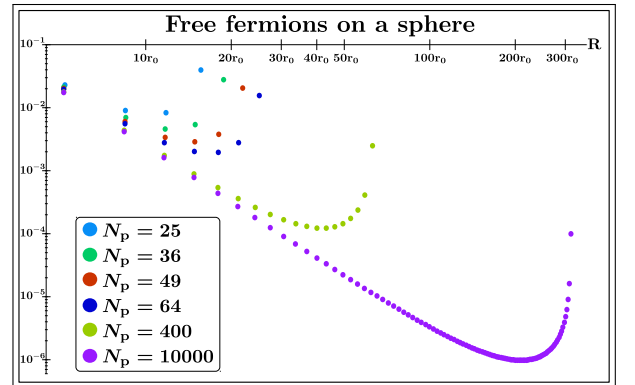


Figure 4. The amplitude of $2k_F$ oscillations exhibited by free fermions on a sphere deviates significantly from the $N_p \rightarrow \infty$ limit (solid line) up to relatively large particle numbers.

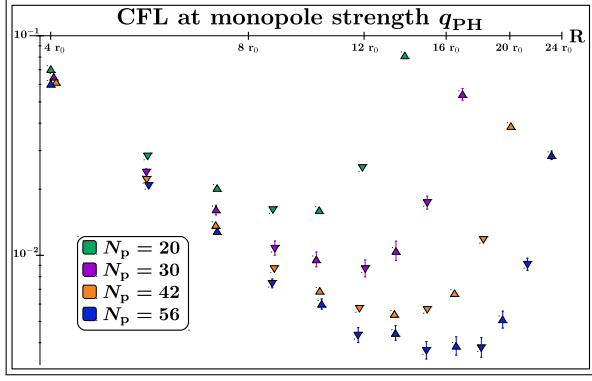


Figure 5. The $2k_F$ oscillations of the CFL at q_P qualitatively match those of free-fermions. Notice that the odd peaks are systematically higher than the even ones, since we show both maxima (up-pointing triangles) and minima (down-pointing triangles), and the base-line is non-constant.

coefficients $A_n^{N_c}$ for $q > 0$ are given by

$$A_n^{N_c} = \sum_{s=n}^{N_c} \sum_{k=n}^s \frac{2(-1)^k [2p(N_p - 1) + 2q + 1 + k - n]!}{n!(s-k)! [2p(N_p - 1) + 2q + 1]!(k-n)!} \times \frac{(s+k+2q)! [k+2(p+q)]!}{(k+2q)! [n+2(p+q)]!} \left[\frac{(pN_p + 2q + 1)!}{(pN_p + k + 2q + 1)!} \right]^2. \quad (\text{C13})$$

Appendix D: Fermi liquids and composite Fermi liquids on a sphere

To help interpret our numerical results for CFLs, it is instructive to recall the free-fermion behavior in the same geometry. At monopole strength $q = 0$, the free-fermion structure factor is given by

$$S_l = 1 - \sum_{l_1, l_2=0}^{l_F} \frac{(2l_1 + 1)(2l_2 + 1)}{4\pi(l_F + 1)^2} \begin{pmatrix} l & l_1 & l_2 \\ 0 & 0 & 0 \end{pmatrix}^2, \quad (\text{D1})$$

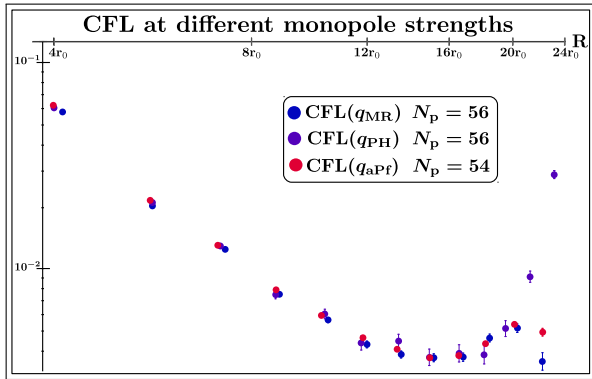


Figure 6. CFLs at different monopole strengths and comparable particle numbers exhibit similar $2k_F$ oscillation apart from the final peak.

Table IV. At $N_p = 56$, the PH-Pfaffian trial wave function with pairwise projection is converged to more than 99% at the cutoff $N_c = l_c - |q| \geq 14$; for single CF projection, the convergence is reached for $N_c \geq 12$.

	$N_c = 12$	$N_c = 14$	$N_c = 15$
$ \langle \Psi_{\text{PH}, N_c=20}^{\text{pair}} \Psi_{\text{PH}, N_c}^{\text{pair}} \rangle $	88.7(2)%	99.42(2)%	99.90(1)%
$ \langle \Psi_{\text{PH}, N_c=20}^{\text{single}} \Psi_{\text{PH}, N_c}^{\text{single}} \rangle $	99.79(1)%	99.980(1)%	99.9994(1)%

where the last term on the right-hand side is the Wigner $3j$ symbol. The amplitudes of the corresponding $2k_F$ oscillations⁷⁰ are shown in Fig. 4. As expected for a gapless state, there are strong finite-size effects. Even for large system sizes inaccessible by Monte Carlo methods, there are significant deviations from the thermodynamic behavior. In particular, the oscillation amplitudes *increase* as $R \rightarrow \pi$, i.e., between antipodal points. A numerically accurate determination of the exponent α is thus challenging.

For the CFLs, we obtained data for up to $N_p = 56$. We find good qualitative agreement with the free fermion behavior (Fig. 5). In particular, the decay of oscillations changes substantially between $N_p = 20$ and $N_p = 56$. Any decay exponent extracted from small to moderate system sizes should thus be viewed as a lower bound on its actual value. Still, our data suggest that α takes a somewhat smaller value than for free fermions in the thermodynamic limit.

We find only a weak dependence of the $2k_F$ oscillation on the monopole strength (Fig. 6). The data for q_{MR} , q_{aPf} , and q_{PH} deviate only very close to $R \approx \pi$. The latter exhibit an upturn that corresponds to constructive interference, similar to the case of free fermions at zero monopole strength. By contrast, there appears to be destructive interference for q_{MR} and q_{aPf} (notice, however, that the final dip is preceded by an increase for $R \gtrsim \pi/2$).

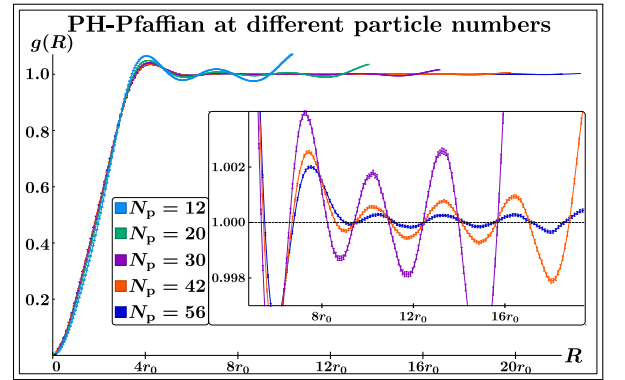


Figure 7. The density-density correlation function of the PH-Pfaffian trial state shows a global suppression of the $2k_F$ amplitudes with increasing particle number, but almost no change in the R dependence.

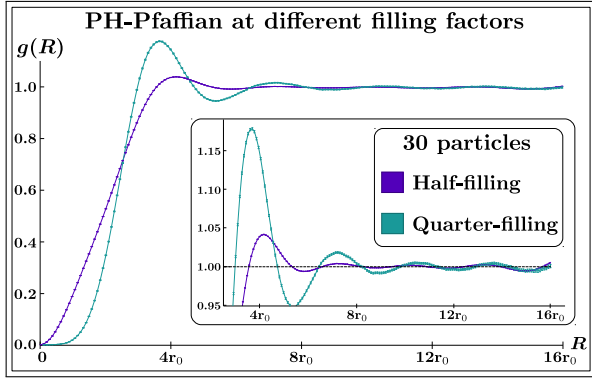


Figure 8. The density-density correlation functions of the PH-Pfaffian with $N_p = 30$ at filling factors $\nu = \frac{1}{4}$ and $\nu = \frac{1}{2}$ are qualitatively similar. At short distances $g(R) \propto R^{2/\nu-2}$, and $2k_F$ oscillations persist for all R .

Appendix E: PH-Pfaffian supplementary data

We show the convergence of the single and pairwise projection methods in Tab. IV. Specifically, we take the pairwise projected state with $N_c = l_c - |q| = 20$ as a reference for $N_p = 56$ and determine the overlap for any smaller cutoff. We find that the convergence is exponentially fast, and an overlap above 99% is reached for $N_c \geq 14$. In general, the cutoff $l_c \approx 2l_F$ provides a good approximation at any particle numbers.

To further characterize the PH-Pfaffian trial state, we show the density-density correlation function for different particle numbers in Fig. 7. The overall R -independent amplitude of oscillations decreases with particle number, but there is no significant difference in the R dependence. For all N_p , the oscillation amplitudes exhibit an increase for $R \gtrsim \pi/2$, similar to free fermions and CFLs [cf. App. D]. Consequently, we may place the bound $\xi_{\text{PH}} > 12r_0$ on the correlation length of the PH-Pfaffian trial state. This value is an order of magnitude larger than those found for the Moore-Read and anti-Pfaffian wave functions.

Finally, we compare the PH-Pfaffian trial states at filling factors $\nu = \frac{1}{2}$ and $\nu = \frac{1}{4}$ for $N_p = 30$ in Fig. 8. In the quarter-filled case, there is a somewhat stronger R dependence of the oscillation amplitude, but at both

fillings, the oscillations persist over the entire sphere. It may be worth exploring whether the R dependence is indicative of an exponential decay at larger N_p , but the correlation length would still be substantially longer than in the case of Moore-Read or anti-Pfaffian.

Appendix F: Anti-Pfaffian entanglement spectra

The trial states $\Psi_{\text{anti-Pfaffian}}^{\text{CF}}$ and $\Psi_{\text{anti-Pfaffian}}$ exhibit overlaps above 99% for $N_p \leq 10$ with the PH-conjugate Moore-Read wave function (see Tab. III). Thus, it is unsurprising that their entanglement spectra⁸² also match well, but we still provide them for completeness. Specifically, we perform an orbital decomposition where subsystem A contains five particles with positive angular momentum L_z and B the other five with negative L_z . In Fig. 9, we plot the corresponding entanglement energies as a function of the total angular momentum in subsystem A . When using pairwise projection, the overlaps with $\Psi_{\text{anti-Pfaffian}}$ are somewhat smaller, but the entanglement spectrum still matches qualitatively; the degeneracies of the low-lying states are identical.

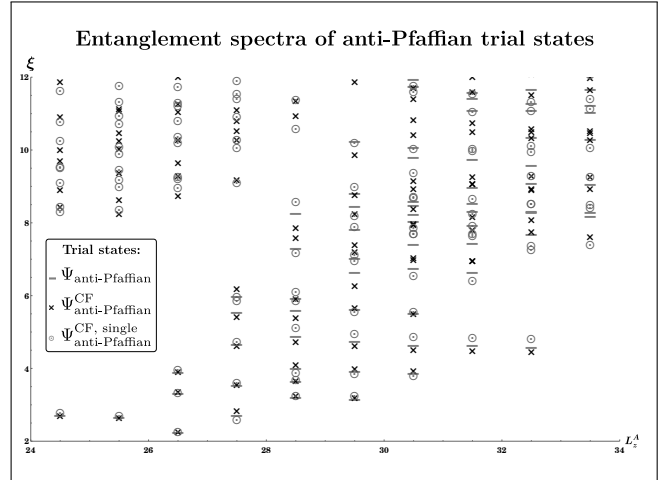


Figure 9. The low-lying states in the orbital entanglement spectra of the trial states $\Psi_{\text{anti-Pfaffian}}^{\text{CF}}$ and $\Psi_{\text{anti-Pfaffian}}^{\text{CF, single}}$ exhibit perfect qualitative agreement with those obtained through PH conjugation of the Moore-Read wave function.

¹ R. L. Willett, R. R. Ruel, K. W. West, and L. N. Pfeiffer, “Experimental demonstration of a Fermi surface at one-half filling of the lowest Landau level,” *Phys. Rev. Lett.* **71**, 3846 (1993).
² W. Kang, H. L. Stormer, L. N. Pfeiffer, K. W. Baldwin, and K. W. West, “How real are composite fermions?” *Phys. Rev. Lett.* **71**, 3850 (1993).
³ V. J. Goldman, B. Su, and J. K. Jain, “Detection of composite fermions by magnetic focusing,” *Phys. Rev. Lett.* **72**, 2065 (1994).

⁴ E. Rezayi and N. Read, “Fermi-liquid-like state in a half-filled Landau level,” *Phys. Rev. Lett.* **72**, 900 (1994).
⁵ J. H. Smet, D. Weiss, R. H. Blick, G. Lütjering, K. von Klitzing, R. Fleischmann, R. Ketzmerick, T. Geisel, and G. Weimann, “Magnetic focusing of composite fermions through arrays of cavities,” *Phys. Rev. Lett.* **77**, 2272 (1996).
⁶ J. K. Jain, “Composite-fermion approach for the fractional quantum Hall effect,” *Phys. Rev. Lett.* **63**, 199 (1989).

- ⁷ J. K. Jain and R. K. Kamilla, “Quantitative study of large composite-fermion systems,” *Phys. Rev. B* **55**, R4895 (1997).
- ⁸ J. K. Jain, *Composite Fermions* (Cambridge University Press, 2007).
- ⁹ B. I. Halperin, P. A. Lee, and N. Read, “Theory of the half-filled Landau level,” *Phys. Rev. B* **47**, 7312 (1993).
- ¹⁰ R. Willett, J. P. Eisenstein, H. L. Störmer, D. C. Tsui, A. C. Gossard, and J. H. English, “Observation of an even-denominator quantum number in the fractional quantum Hall effect,” *Phys. Rev. Lett.* **59**, 1776 (1987).
- ¹¹ R. H. Morf, “Transition from quantum Hall to compressible states in the second Landau level: new light on the $\nu = 5/2$ enigma,” *Phys. Rev. Lett.* **80**, 1505 (1998).
- ¹² E. H. Rezayi and F. D. M. Haldane, “Incompressible paired Hall state, stripe order, and the composite fermion liquid phase in half-filled Landau levels,” *Phys. Rev. Lett.* **84**, 4685 (2000).
- ¹³ A. Wójs, C. Toke, and J. K. Jain, “Landau-level mixing and the emergence of Pfaffian excitations for the $5/2$ fractional quantum Hall effect,” *Phys. Rev. Lett.* **105**, 096802 (2010).
- ¹⁴ M. Storni, R. H. Morf, and S. Das Sarma, “Fractional quantum Hall state at $\nu = 5/2$ and the Moore-Read Pfaffian,” *Phys. Rev. Lett.* **104**, 076803 (2010).
- ¹⁵ A. E. Feiguin, E. Rezayi, C. Nayak, and S. Das Sarma, “Density matrix renormalization group study of incompressible fractional quantum Hall states,” *Phys. Rev. Lett.* **100**, 166803 (2008).
- ¹⁶ A. E. Feiguin, E. Rezayi, K. Yang, C. Nayak, and S. Das Sarma, “Spin polarization of the $\nu = 5/2$ quantum Hall state,” *Phys. Rev. B* **79**, 115322 (2009).
- ¹⁷ M. R. Peterson, Th. Jolicoeur, and S. Das Sarma, “Finite-layer thickness stabilizes the Pfaffian state for the $5/2$ fractional quantum Hall effect: Wave function overlap and topological degeneracy,” *Phys. Rev. Lett.* **101**, 016807 (2008).
- ¹⁸ E. H. Rezayi and S. H. Simon, “Breaking of particle-hole symmetry by Landau level mixing in the $\nu = 5/2$ quantized Hall state,” *Phys. Rev. Lett.* **106**, 116801 (2011).
- ¹⁹ K. Pakrouski, M. R. Peterson, Th. Jolicoeur, V. W. Scarola, C. Nayak, and M. Troyer, “Phase diagram of the $\nu = 5/2$ fractional quantum Hall effect: Effects of Landau-level mixing and nonzero width,” *Phys. Rev. X* **5**, 021004 (2015).
- ²⁰ B. I. Halperin, “Theory of the quantized Hall conductance,” *Helv. Phys. Acta* **56**, 75 (1983).
- ²¹ G. Moore and N. Read, “Nonabelions in the fractional quantum Hall effect,” *Nucl. Phys. B* **360**, 362 (1991).
- ²² M. Greiter, X. G. Wen, and F. Wilczek, “Paired Hall state at half filling,” *Phys. Rev. Lett.* **66**, 3205 (1991).
- ²³ F. D. M. Haldane and E. H. Rezayi, “Spin-singlet wave function for the half-integral quantum Hall effect,” *Phys. Rev. Lett.* **60**, 956 (1988).
- ²⁴ N. Read and D. Green, “Paired states of fermions in two dimensions with breaking of parity and time-reversal symmetries and the fractional quantum Hall effect,” *Phys. Rev. B* **61**, 10267 (2000).
- ²⁵ M. Levin, B. I. Halperin, and B. Rosenow, “Particle-hole symmetry and the Pfaffian state,” *Phys. Rev. Lett.* **99**, 236806 (2007).
- ²⁶ S. S. Lee, S. Ryu, C. Nayak, and M. P. A. Fisher, “Particle-hole symmetry and the $\nu = 5/2$ quantum Hall state,” *Phys. Rev. Lett.* **99**, 236807 (2007).
- ²⁷ S. M. Girvin, “Particle-hole symmetry in the anomalous quantum Hall effect,” *Phys. Rev. B* **29**, 6012 (1984).
- ²⁸ D. T. Son, “Is the composite Fermion a Dirac particle?” *Phys. Rev. X* **5**, 031027 (2015).
- ²⁹ M. A. Metlitski and A. Vishwanath, “Particle-vortex duality of two-dimensional Dirac fermion from electric-magnetic duality of three-dimensional topological insulators,” *Phys. Rev. B* **93**, 245151 (2016).
- ³⁰ C. Wang and T. Senthil, “Half-filled Landau level, topological insulator surfaces, and three-dimensional quantum spin liquids,” *Phys. Rev. B* **93**, 085110 (2016).
- ³¹ S. D. Geraedts, M. P. Zaletel, R. S. K. Mong, M. A. Metlitski, A. Vishwanath, and O. I. Motrunich, “The half-filled Landau level: The case for Dirac composite fermions,” *Science* **352**, 197 (2016).
- ³² G. Murthy and R. Shankar, “ $\nu = 1/2$ Landau level: Half-empty versus half-full,” *Phys. Rev. B* **93**, 085405 (2016).
- ³³ S. Kachru, M. Mulligan, G. Torroba, and H. Wang, “Mirror symmetry and the half-filled Landau level,” *Phys. Rev. B* **92**, 235105 (2015).
- ³⁴ D. F. Mross, J. Alicea, and O. I. Motrunich, “Explicit derivation of duality between a free Dirac cone and quantum electrodynamics in $(2 + 1)$ dimensions,” *Phys. Rev. Lett.* **117**, 016802 (2016).
- ³⁵ M. Mulligan, S. Raghu, and M. P. A. Fisher, “Emergent particle-hole symmetry in the half-filled Landau level,” *Phys. Rev. B* **94**, 075101 (2016).
- ³⁶ A. C. Balam and J. K. Jain, “Nature of composite fermions and the role of particle-hole symmetry: A microscopic account,” *Phys. Rev. B* **93**, 235152 (2016).
- ³⁷ J. Yang, “Dirac composite fermion - A particle-hole spinor,” [arXiv:1711.08520](https://arxiv.org/abs/1711.08520) (2017).
- ³⁸ M. Fremling, N. Moran, J. K. Slingerland, and S. H. Simon, “Trial wave functions for a composite Fermi liquid on a torus,” *Phys. Rev. B* **97**, 035149 (2018).
- ³⁹ X. Chen, L. Fidkowski, and A. Vishwanath, “Symmetry enforced non-Abelian topological order at the surface of a topological insulator,” *Phys. Rev. B* **89**, 165132 (2014).
- ⁴⁰ P. Bonderson, C. Nayak, and X. L. Qi, “A time-reversal invariant topological phase at the surface of a 3D topological insulator,” *J. Stat. Mech.* **2013**, P09016 (2013).
- ⁴¹ M. A. Metlitski, C. L. Kane, and M. P. A. Fisher, “Symmetry-respecting topologically ordered surface phase of three-dimensional electron topological insulators,” *Phys. Rev. B* **92**, 125111 (2015).
- ⁴² C. Wang, A. C. Potter, and T. Senthil, “Gapped symmetry preserving surface state for the electron topological insulator,” *Phys. Rev. B* **88**, 115137 (2013).
- ⁴³ D. F. Mross, A. Essin, and J. Alicea, “Composite Dirac liquids: Parent states for symmetric surface topological order,” *Phys. Rev. X* **5**, 011011 (2015).
- ⁴⁴ M. Dolev, M. Heiblum, V. Umansky, A. Stern, and D. Mahalu, “Observation of a quarter of an electron charge at the $\nu = 5/2$ quantum Hall state,” *Nature (London)* **452**, 829 (2008).
- ⁴⁵ M. Banerjee, M. Heiblum, V. Umansky, D. E. Feldman, Y. Oreg, and A. Stern, “Observation of half-integer thermal Hall conductance,” *Nature (London)* **559**, 205 (2018).
- ⁴⁶ D. F. Mross, Y. Oreg, A. Stern, G. Margalit, and M. Heiblum, “Theory of disorder-induced half-integer thermal Hall conductance,” *Phys. Rev. Lett.* **121**, 026801 (2018).
- ⁴⁷ B. Lian and J. Wang, “Theory of the disordered $\nu = 5/2$ quantum thermal Hall state: Emergent symmetry and

- phase diagram,” *Phys. Rev. B* **97**, 165124 (2018).
- ⁴⁸ C. Wang, A. Vishwanath, and B. I. Halperin, “Topological order from disorder and the quantized Hall thermal metal: Possible applications to the $\nu = 5/2$ state,” *Phys. Rev. B* **98**, 045112 (2018).
- ⁴⁹ S. H. Simon, “Interpretation of thermal conductance of the $\nu = 5/2$ edge,” *Phys. Rev. B* **97**, 121406(R) (2018).
- ⁵⁰ D. E. Feldman, “Comment on ‘interpretation of thermal conductance of the $\nu = 5/2$ edge’,” *Phys. Rev. B* **98**, 167401 (2018).
- ⁵¹ S. H. Simon, “Reply to ‘Comment on ‘Interpretation of thermal conductance of the $\nu = 5/2$ edge’ ’,” *Phys. Rev. B* **98**, 167402 (2018).
- ⁵² K. K. W. Ma and D. E. Feldman, “Partial equilibration of integer and fractional edge channels in the thermal quantum Hall effect,” *Phys. Rev. B* **99**, 085309 (2019).
- ⁵³ S. H. Simon and B. Rosenow, “Partial equilibration of the anti-Pfaffian edge due to Majorana disorder,” *Phys. Rev. Lett.* **124**, 126801 (2020).
- ⁵⁴ Hamed Asasi and Michael Mulligan, “Partial equilibration of anti-pfaffian edge modes at $\nu = 5/2$,” *Phys. Rev. B* **102**, 205104 (2020).
- ⁵⁵ P. T. Zucker and D. E. Feldman, “Stabilization of the particle-hole Pfaffian order by Landau-level mixing and impurities that break particle-hole symmetry,” *Phys. Rev. Lett.* **117**, 096802 (2016).
- ⁵⁶ J. Yang, “Particle-hole symmetry and the fractional quantum Hall states at $5/2$ filling factor,” [arXiv:1701.03562](https://arxiv.org/abs/1701.03562) (2017).
- ⁵⁷ Th. Jolicœur, “Non-abelian states with negative flux: A new series of quantum hall states,” *Phys. Rev. Lett.* **99**, 036805 (2007).
- ⁵⁸ A. C. Balram, M. Barkeshli, and M. S. Rudner, “Parton construction of a wave function in the anti-Pfaffian phase,” *Phys. Rev. B* **98**, 035127 (2018).
- ⁵⁹ R. V. Mishmash, D. F. Mross, J. Alicea, and O. I. Motrunich, “Numerical exploration of trial wave functions for the particle-hole-symmetric Pfaffian,” *Phys. Rev. B* **98**, 081107(R) (2018).
- ⁶⁰ G. Möller and S. H. Simon, “Paired composite-fermion wave functions,” *Phys. Rev. B* **77**, 075319 (2008).
- ⁶¹ Gunnar Möller, *Dynamically reduced spaces in condensed matter physics: jbr /¿Quantum Hall bilayers, dimensional reduction, and magnetic spin systems*, *Theses*, Université Paris Sud - Paris XI (2006).
- ⁶² X. G. Wen and A. Zee, “Shift and spin vector: New topological quantum numbers for the Hall fluids,” *Phys. Rev. Lett.* **69**, 953 (1992).
- ⁶³ Monopole harmonics and their properties were described in Refs. 78 and 79; we use the conventions of Ref. 8.
- ⁶⁴ Gunnar Möller, Steven H. Simon, and Edward H. Rezayi, “Trial wave functions for $\nu = \frac{1}{2} + \frac{1}{2}$ quantum hall bilayers,” *Phys. Rev. B* **79**, 125106 (2009).
- ⁶⁵ J. Wang, S. D. Geraedts, E. H. Rezayi, and F. D. M. Haldane, “Lattice Monte Carlo for quantum Hall states on a torus,” *Phys. Rev. B* **99**, 125123 (2019).
- ⁶⁶ S. C. Davenport and S. H. Simon, “Spinful composite fermions in a negative effective field,” *Phys. Rev. B* **85**, 245303 (2012).
- ⁶⁷ J. Fulsebakke, “Projections and correlations in the fractional quantum Hall effect,” *Ph.D. thesis* (2016).
- ⁶⁸ S. Mukherjee and S. S. Mandal, “Incompressible states of the interacting composite fermions in negative effective magnetic fields at $\nu = 4/13, 5/17$, and $3/10$,” *Phys. Rev. B* **92**, 235302 (2015).
- ⁶⁹ Upon rewriting Eq. (5) in the form of Eq. (B6a), it becomes manifest that the pairing channel is unaffected by truncating the infinite sum.
- ⁷⁰ The structure factor is related to the real-space correlation function via $g(R) = 1 + \frac{4\pi}{N_p} \sum_l \frac{2l+1}{4\pi} (S_l - 1) P_l[\cos(R)]$. In spherically symmetric cases, our definition coincides with that of Ref. 77.
- ⁷¹ B. L. Altshuler, L. B. Ioffe, and A. J. Millis, “Low-energy properties of fermions with singular interactions,” *Phys. Rev. B* **50**, 14048 (1994).
- ⁷² D. F. Mross, J. McGreevy, H. Liu, and T. Senthil, “Controlled expansion for certain non-Fermi-liquid metals,” *Phys. Rev. B* **82**, 045121 (2010).
- ⁷³ D. N. Sheng, O. I. Motrunich, and M. P. A. Fisher, “Spin Bose-metal phase in a spin- $\frac{1}{2}$ model with ring exchange on a two-leg triangular strip,” *Phys. Rev. B* **79**, 205112 (2009).
- ⁷⁴ Gunnar Möller, Arkadiusz Wójs, and Nigel R. Cooper, “Neutral fermion excitations in the moore-read state at filling factor $\nu = 5/2$,” *Phys. Rev. Lett.* **107**, 036803 (2011).
- ⁷⁵ P. Bonderson, A. E. Feiguin, and C. Nayak, “Numerical calculation of the neutral fermion gap at the $\nu = 5/2$ fractional quantum Hall state,” *Phys. Rev. Lett.* **106**, 186802 (2011).
- ⁷⁶ M. Baraban, G. Zikos, N. Bonesteel, and S. H. Simon, “Numerical analysis of quasiholes of the Moore-Read wave function,” *Phys. Rev. Lett.* **103**, 076801 (2009).
- ⁷⁷ R. K. Kamilla, J. K. Jain, and S. M. Girvin, “Fermi-sea-like correlations in a partially filled Landau level,” *Phys. Rev. B* **56**, 12411 (1997).
- ⁷⁸ T. T. Wu and C. N. Yang, “Dirac monopole without strings: Monopole harmonics,” *Nucl. Phys. B* **107**, 365 (1976).
- ⁷⁹ T. T. Wu and C. N. Yang, “Some properties of monopole harmonics,” *Phys. Rev. D* **16**, 1018 (1977).
- ⁸⁰ One can always find a conformal transformation that maps \mathbf{r}_a and \mathbf{r}_b to opposite poles and thus $h_i \rightarrow u_i/v_i$, while the cross-ratio $\omega_{ab}\Omega_{ij}$ is conformally invariant.
- ⁸¹ M. Wimmer, “Algorithm 923: Efficient numerical computation of the Pfaffian for dense and banded skew-symmetric matrices,” *ACM Trans. Math. Softw.* **38** (2012), 10.1145/2331130.2331138.
- ⁸² H. Li and F. D. M. Haldane, “Entanglement spectrum as a generalization of entanglement entropy: Identification of topological order in non-Abelian fractional quantum Hall effect states,” *Phys. Rev. Lett.* **101**, 010504 (2008).